RESEARCH PAPER

Corrosion Behavior of API 5L X70 Carbon Steels in Hydrogen Sulfide Environments

Jonas Fernando Macedo, Igor Alexandre Fioravante, Roberto Zenhei Nakazato, Heloisa Andréa Acciari and Eduardo Norberto Codaro *

* *eduardo.codaro@unesp.br*

Received: September 2020 Revised: November 2020 Accepted: December 2020

São Paulo State University (UNESP), School of Engineering, Guaratinguetá, SP, Brazil

DOI: 10.22068/ijmse.18.1.12

Abstract: *As we all know, corrosion of pipelines by hydrogen sulfide is the most worrying factor in the production and transport of oil and gas. In this work the corrosion behavior of API 5L X70MS and X70MO low carbon steels in hydrogen sulfide environment was investigated. Hydrogen induced cracking and sulfide stress cracking tests were carried out according to NACE TM0177 standard. After testing, blisters and cracks were observed only in X70MO steel, probably due to its lower grain refinement and banded microstructure. Internal cracks seem to be initiated in the elongated MnS inclusions. Corrosion process was studied by obtaining potentiodynamic polarization curves, which were registered after open circuit potential measurements, at room temperature. Both steels showed general corrosion in NACE 177A solutions, but the corrosion rate values in H_2S-saturated solution were about an order of magnitude higher than the ones in deaerated solution. Hydrogen permeation was characterized in accordance with ASTM G148 standard. In deaerated H_2SO_4 solution, permeation measurements were similar for both steels. In H_2S-saturated solution, X70 MO exhibited higher hydrogen oxidation current values than X70 MS. H_2S seems to promote the reduction of protons and increase the concentration of hydrogen atoms in the solution/steel interface, favoring the diffusion process. As X70MO has a coarse microstructure, it offers more pathways for hydrogen diffusion.*

Keywords: *X70 steel, Hydrogen induced cracking, Sulfide stress cracking, Sour corrosion, Low carbon steel.*

1. INTRODUCTION

Sour corrosion has always been a concern for the oil and natural gas exploration and production industries. It causes loss or contamination of product, reduction in operational efficiency and refinery shutdowns. Pipe repair and replacement costs tend to increase as more hostile environments and more aggressive oils are found. Low carbon steels are the most commonly used materials because these are readily available in the market and can meet many of the mechanical, manufacturing and cost requirements [1,2]. However, these steels have relatively low corrosion resistance and pipelines may undergo general or localized corrosion, depending on steel composition and microstructure, oil composition and operating conditions such as pressure, temperature and fluid dynamics. General corrosion is a consequence of preferential dissolution of the predominant phase (e.g. ferritic phase) and may be manifested by increased surface roughness or the formation of a scale composed mainly of iron sulfides [3,4]. Localized corrosion arises from the existence of galvanic pairs formed between the predominant phase and the non-metallic (e.g. MnS) or intermetallic (e.g. Fe_3C) inclusions [5], and it commonly manifests as pitting or mesa attack [6,7]. Hydrogen embrittlement is another form of localized corrosion, in which a fraction of the hydrogen atoms generated by steel corrosion diffuses from the surface to the steel, accumulating in traps. These traps can be point defects (vacancies), line defects (dislocations), two-dimensional defects (grain boundaries and triple grain junction) and discontinuities (pores and boundaries of intermetallic particles such as Fe_3C, non-metallic inclusions such as MnS, and impurities as oxides). Then hydrogen atoms can react with each other to form hydrogen gas or they can react with different atoms to form metal hydrides, decreasing the lattice energy (decohesion). After that, the formation of hydrogen gas leads to pressurization of these traps, causing residual stress, blistering and internal cracking [8-10]. Although corrosion consequences are known, causes and mechanisms by which this phenomenon occurs are still not well understood. There are two

contributing factors to this situation, which are: a correlation of multiple parameters (metallurgical and environmental variables) that influence corrosion and the limitations of laboratory test systems to reproduce the internal conditions of pipelines [11,12]. As the chemical compositions of petroleum, natural gas and produced water vary widely, standard corrosion tests have been developed to evaluate the cracking resistance of carbon steels. These tests establish specific conditions for sample, solution, H_2S partial pressure, temperature and exposure time. Researches using different electrochemical techniques in aqueous media have also made a significant contribution in this sense. Artificial sea water and other saline solutions containing different concentrations of hydrogen sulfide have often been used as corrosive media, probably because these media having a similar chemical composition to emulsified water in oil [13-15]. In the last decades, microalloyed steels with transition metals were developed to obtain higher mechanical properties, aiming at the manufacture of pipes of smaller thickness and lower weight/length ratio. However, steel pipes produced by thermomechanical processes may have different microstructures depending on the processing conditions [16,17] and therefore require qualification testing for use in sour environments. Considering that the understanding the metallurgical factors is of great importance to minimize and control corrosion problem in oil industries, the aim of the study was to investigate the effects of composition and microstructure on corrosion processes involving API 5L X70 high strength steels in NACE 177A solution.

2. MATERIALS AND METHODS

API 5L X70MO and X70MS steels pipes are commonly manufactured in Brazil. The former is used in off-shore environments, whereas the latter is produced to resist harsh sour conditions. Both pipes were manufactured according to standard specification for steel line pipe [18] through the cold forming process by three-stage pressing (edge pressing, U-shaped pressing and O-shaped pressing), followed by longitudinal submerged arc welding, and expansion in order to calibrate the final geometry of pipes. Samples of 100×20×10 mm and 130×20×5 mm were taken from the 558.8 mm pipes by plasma cutting at approximately 90 and 180 degrees from the longitudinal weld. Chemical composition of these samples (Table 1) was determined by optical emission spectrometry with a Thermo ARL 3460 spectrometer and the ARL WinOE software.

The hydrogen-induced cracking (HIC) test consists of exposing unstressed samples to a specific standard solution. On the other hand, in the sulfide stress cracking (SSC) test, the samples are subjected to a tensile stress using a constant deflection device (four point bend test) [19] and then exposed to the standard solution. To evaluate HIC and SSC resistances of these steels, two vessels were used for each test (Fig. 1), one containing 10 L of 5.0 wt.% NaCl + 0.5 wt.% CH_3COOH standard solution [20,21] and the other one containing 12 samples (6 X70MS + 6 X70MO) previously polished with 600 mesh emery paper and degreased with isopropyl alcohol. A screwed cap and a rubber gasket ring were used to hermetically close both vessels. One inlet valve was used to inject gas into the solution preparation vessel and two outlet valves were used to transfer gas and solution to the test vessel, respectively. Before transferring the standard solution into the test vessel, it was purged of air with $N_{2(g)}$ 99.999% for 1 h at 100 mL/min per liter of solution and then saturated with $H_2S_{(g)}$ 99.9% at the same flow rate. To ensure that this solution remained saturated, $H_2S_{(g)}$ was continuously injected during the test. Both HIC and SSC tests were performed at 24 ± 3 ˚C.

Table 1. Chemical composition of API 5L X70MS and API 5L X70MO steels (wt. %).

X70	C	S	Al	P	Si	Cr	Mn	Ni	Cu	Mo	Others
MS	0.028	0.0006	0.02	0.011	0.30	0.180	1.29	0.170	0.150	0.14	**a**
MO	0.096	0.0015	0.03	0.018	0.28	0.027	1.62	0.014	0.016	0.004	**b**

a Ti = 0.008%; V = 0.050%; Nb = 0.034%; Ca = 0.0020%

b Ti = 0.014%; V = 0.003%; Nb = 0.044%; Ca = 0.0015%

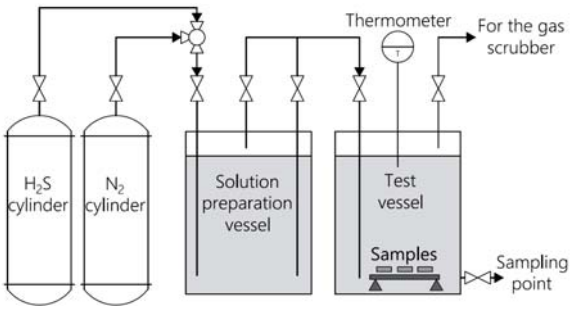

Fig. 1. HIC and SSC test apparatus.

Metallographic analysis using a Zeiss Observer Z1M inverted microscope with AxioVision image analysis software was employed in this work. The microstructures were revealed by chemical etching with 3.0% Nital. The surfaces and cross sections of samples were examined using a Jeol 6350 scanning electron microscope, and the composition of phases was determined using X-ray dispersive energy spectrometry (Thermo C10015 probe controlled by the Noran System SIX software).

Open circuit potential (OCP) and potentiodynamic measurements were carried out in a conventional three-electrode cell coupled to an Autolab PGSTAT302N potentiostat/ galvanostat. Steel sheets were used as working electrodes and a spiral-shaped Pt wire was the counter electrode. Before each electrochemical measurement, the steel sheet was mechanically polished with emery papers of different grit sizes from 180 to 600. All potentials were measured taking a saturated Ag/AgCl electrode as a reference. The potentiodynamic measurements were registered at a scan rate of 0.16 mV s^{-1} from the open circuit potential at steady-state. On the other hand, hydrogen permeation experiments were conducted with a Devanathan-Stachurski cell [22], which is composed of two glass compartments separated by the working electrode. Before the measurements, a nickel thin film was electrodeposited on one side of steel sheet (the side of the working electrode in the cell oxidation) precisely to avoid oxidation of the steel. The cathodic compartment consisted of a 0.05 mol L^{-1} H_2SO_4 solution with the addition of 3.0 g L^{-1} of NH_4SCN as a hydrogen adsorption promoter. In this compartment, hydrogen ions were reduced by applying a current of 5.0 mA cm^{-2} using a KEYSIGHT E3643A power supply. In the anodic compartment, hydrogen atoms were oxidized at a constant potential (+0.250 V *vs.* Ag/AgCl) and the anodic current was recorded via the potentiostat. Prior to hydrogen permeation measurements, the electrolyte was deaerated by purging $N_{2(g)}$ for 1 h at 50 mL min^{-1}, and subsequently saturated with $H_2S_{(g)}$ at the same flow rate, at room temperature.

3. RESULTS AND DISCUSSION

3.1. Metallographic Analysis

Figure 2 shows the optical micrographs for additional information on microstructural differences comparing both steels. X70MS steel surface analysis (Fig. 2(a)) revealed a ferritic matrix composed of randomly oriented polygonal grains (light areas) and intergranular pearlite (black spots). The high grain refinement is resulting from the low carbon content, and the thermomechanical treatment (controlled rolling and accelerated cooling) [23]. X70MO steel (Fig. 2(b)) shown a coarse grained ferritic microstructure with the presence of bands (identified by the darker areas). Banding is mainly caused by the microsegregation of alloying elements during steel solidification. Subsequent hot work operations result in an alignment of microsegregation in the work direction, which results in the emergence of outlined bands in the microstructure. In this case, the banding can be a consequence of two factors: high carbon, phosphorus, sulfur and manganese contents in the steel composition and a conventional rolling. Microstructures like this are prone to crack nucleation and propagation by promoting the diffusion and trapping of hydrogen in steel [24].

3.2. Non-electrochemical Tests

HIC test was performed to assess the susceptibility of steels to hydrogen induced cracking at room temperature. X70MS steel did not show any cracks or bubbles after the HIC test (Fig. 3(a)). On the other hand, all the X70MO steel samples presented blisters, as shown in Fig. 3(b).

Internal cracks were detected in X70MO steel by using of a light microscope at 100X (Fig. (4)). Most cracks in this steel are located in the central region of pipe thickness (Fig. 4(a)), where there is band formation and higher concentration of inclusions (Fig. 4(b)).

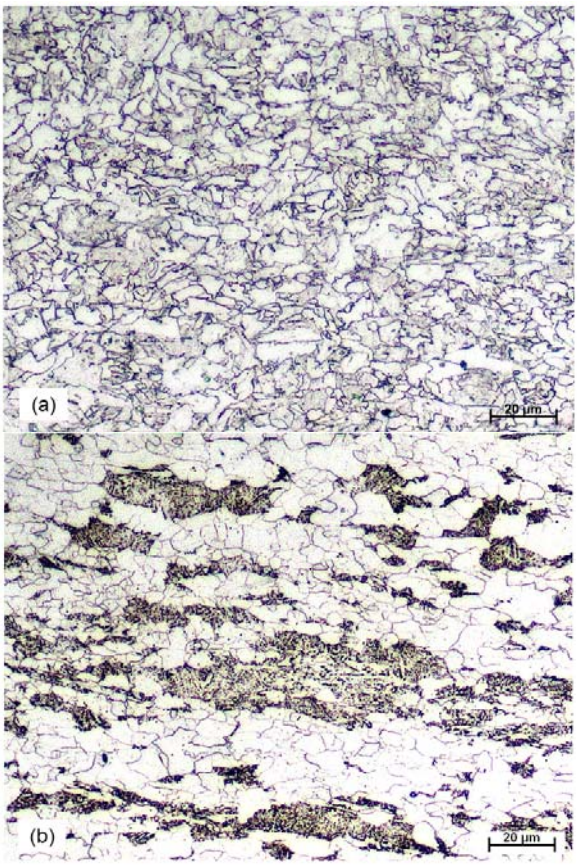

Fig. 2. Optical micrographs of (a) X70MS and (b) X70MO steels.

Fig. 3. (a) X70MS and (b) X70MO after HIC test in NACE 177A Solution.

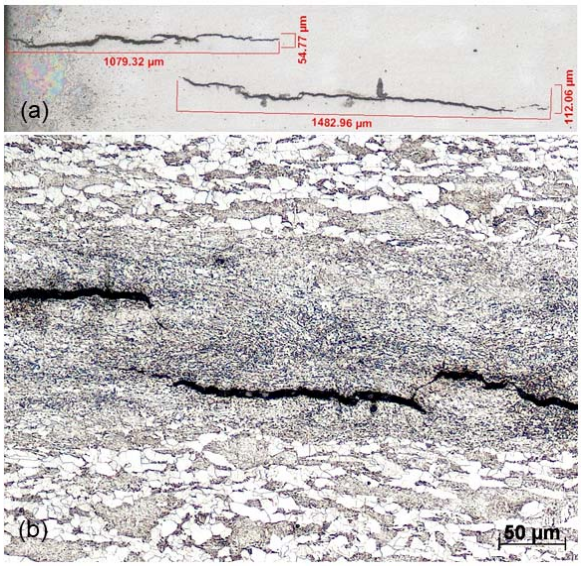

Fig. 4. Internal cracks in X70MO (a) in cross section of pipe and (b) in banded microstructure.

Table 2 lists the mean values of the following parameters: CLR (crack length ratio), CTR (crack thickness ratio), and CSR (crack sensitivity ratio), positioned at 90° and 180° from the weld fillet location. Based on acceptance criteria defined by international standard [25], X70MO steel exhibited CLR values higher than 15% and therefore this steel is not qualified for sour service.

Table 2. HIC test results.

Steel	Position	CLR (%)	CTR (%)	CSR (%)
X70MS	90°	0.0	0.0	0.0
	180°	0.0	0.0	0.0
X70MO	90°	37.0	2.8	1.3
	180°	64.9	1.7	1.6

SEM micrograph in Figure 5(a) shows some cracks in the banded region. EDS analysis in Figure 5(b) revealed the presence of S and Mn within a crack, probably nucleated by an inclusion of MnS [26].

The SSC test aimed to evaluate the susceptibility to cracking of tensile steels when immersed in the test solution. After testing, X70MS steel surface analysis did not reveal the presence of cracks or blisters (Fig. 6). In all samples, an increase in surface roughness due to general corrosion was observed.

Surface analysis of X70MO steel showed intense

attack and blisters formation on the frontal region of the samples (Figures 7(a) and (b)). On the side view (Figure 7(c)), it is also possible to observe a strong plastic deformation in the tested samples and some cracks in their central regions, where the deflection was maximum.

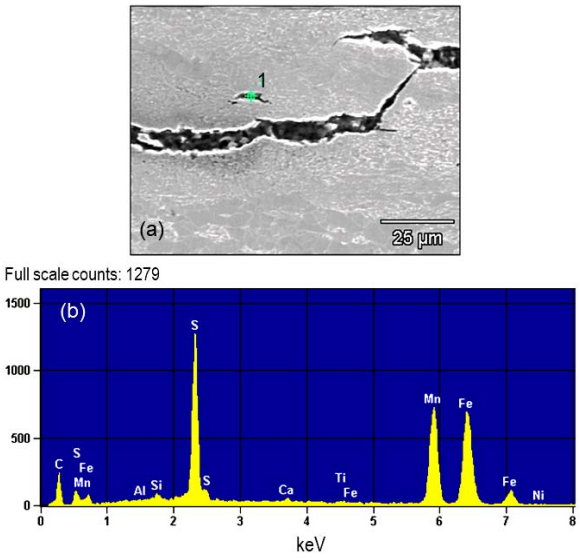

Fig. 5. (a) SEM showing cracks in X70MO steel and (b) EDS analysis in point 1 of Fig. 5(a).

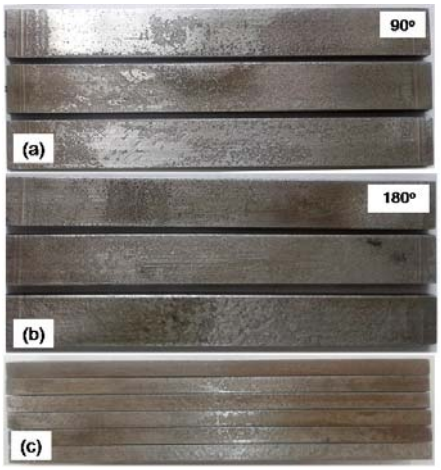

Fig. 6. X70MS steel surface after SSC test: front (a, b) and side (c) view.

Differences in toughness of X70MS and X70MO (Figs. 6(c) and 7(c)) can be attributed to the equivalent carbon content, particularly, the carbon content (Table 1). It is well-known that a high content of equivalent carbon impairs the toughness, so other ways to improve the mechanical strength of carbon steels are needed. Decreasing carbon content as well as the addition of alloying elements are not always enough to ensure high toughness, and therefore, controlled lamination is required.

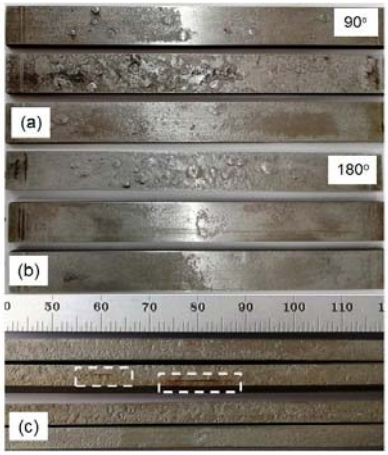

Fig. 7. X70MO steel surface after SSC test: front (a, b) and side view showing cracks (c).

3.3. Electrochemical Tests

The OCP behavior of the X70 steels in NACE 177A solutions was slightly different, according to Figs. 8(a) and (b). The OCP values of X70MS decreased, increased and stabilized and the OCP ones of X70MO increased and then stabilized. The potential variation during the first minutes of immersion depends on the initial state of the electrode surface and on neighboring medium around to it. After this short period, there is a gradual shift in potential towards steady state. The fact that the potential does not vary very much with time suggests that there is no significant change in the polarization of the anodic and cathodic reactions with time. Considering that the lower the value of stabilization potential, the more intense is the corrosive attack, it is possible to conclude that the solution saturated with H_2S is more aggressive than the deaerated solution.

A typical behavior associated with general corrosion was observed in the polarization curves, as shown in Figs. 9(a) and (b). The cathodic branch represents the reduction of protons, which is more efficient in the presence of H_2S. On the other hand, the anodic branch is related to the active dissolution of iron, since neither $Fe(OH)_2$, Fe_2O_3 nor FeS are thermodynamically stable in chloride solutions at pH ≤ 2.7 [27,28].

It is interesting to note that in intermediate anodic overpotentials there is an increase in the dissolution rate of steels in deaerated solution. This fact can be attributed to the formation of

iron intermediary complexes [29] which change

the dissolution mechanism. At high anodic overpotentials (> -0.35 V) the dissolution rates tend to be the same in both solutions, probably due to the formation of corrosion products that limit the passage of species to and from the electrode surface. Another important feature is the general appearance of the curves, which suggests that NACE 177A solutions are so aggressive that differences in composition and microstructure between the steels are not relevant. Table 3 shows corrosion parameters calculated from polarization curves. In both steels, the corrosion potential (E_{corr}) is in agreement with the open circuit potential at steady-state. If an interfacial charge transfer process control the corrosion rate, typical values for Tafel coefficients are between 0.040 and 0.120 V dec^{-1}, depending on the chloride concentration and pH of the solution [30-32]. In this sense, values between 0.060 and 0.100 V dec^{-1} have often been reported for the anodic Tafel coefficient (βa) for iron dissolution in deaerated acidic chloride solutions [32-35].

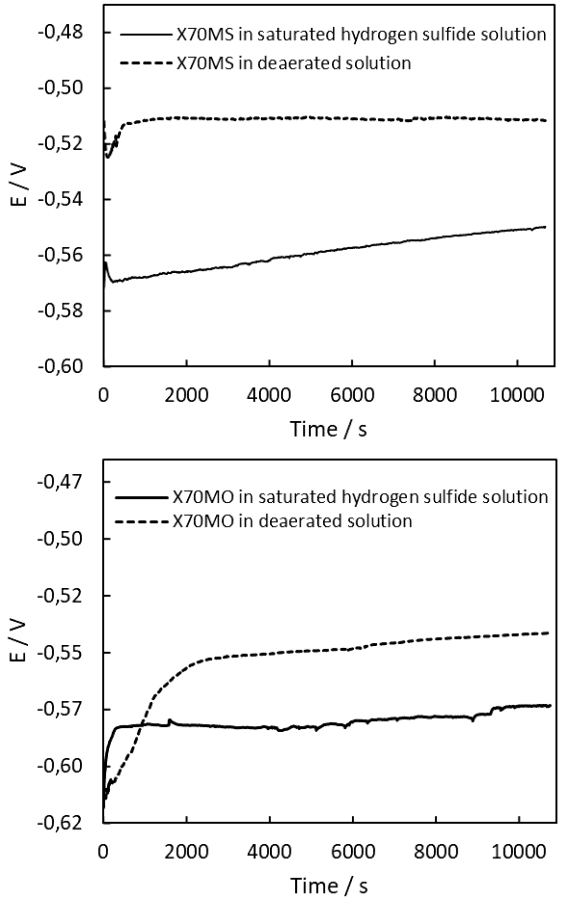

Fig. 8. OCP curves obtained for X70MS (a) and X70MO (b) steels in NACE 177A solutions.

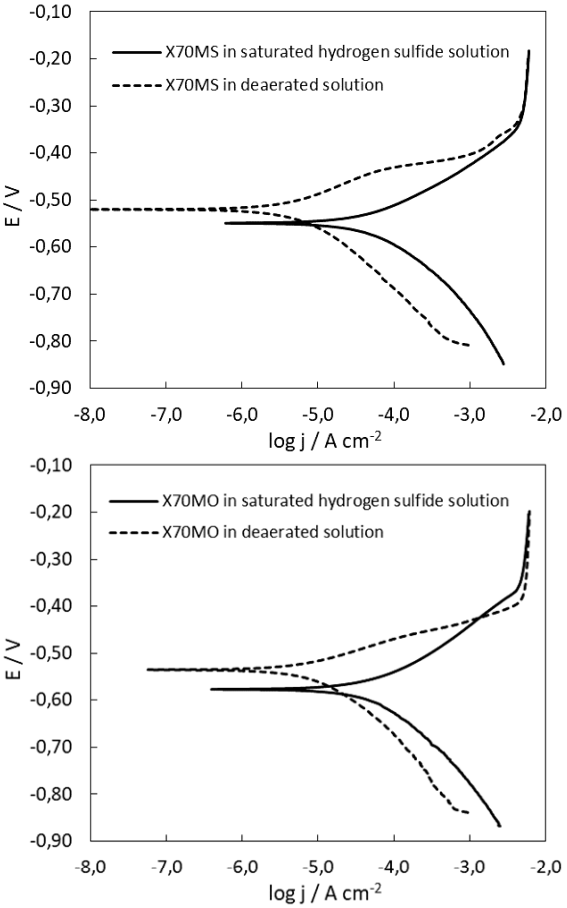

Fig. 9. Polarization curves of X70MS (a) and X70MO (b) steels in NACE 177A solutions.

Table 3. Corrosion parameters of X70 steels in NACE 177A solutions.

Steel	Solution	E_{corr} (V)	j_{corr} (μA cm^{-2})	βa (V dec^{-1})	βc (V dec^{-1})
X70MS	N_2-deaerated	-0.519	4.6	0.061	-0.127
	H_2S-saturated	-0.551	42	0.086	-0.116
X70MO	N_2-deaerated	-0.536	7.0	0.041	-0.119
	H_2S-saturated	-0.578	46	0.097	-0.129

In addition, the corrosion current density (j_{corr}) values in H_2S-saturated solutions were about an order of magnitude higher than those calculated in deaerated solutions. This behavior suggests that the presence of sulfide alters the reaction mechanism at the electrode interface, causing a faster reduction of protons and consequently a higher corrosion rate. The same behavior was

observed with other API 5L steels in acidic media, as previously reported by other authors [36].

The mechanisms of iron dissolution in strongly acid medium have been extensively studied, one of which may explain the corrosion of low carbon steels [37-40]. When low carbon steel is exposed to a sour environment, it is initially corroded and $Fe^{2+}_{(aq)}$ and $H_{2(g)}$ are the main corrosion products. Secondary phases such as cementite or other carbides can act as cathodes, whereas iron dissolution occurs in ferrite grains [37]. In strongly acidic media, iron corrosion probably occurs by means of an adsorbed Fe(II)-hydroxo complex and the oxidation this species is deemed to be the rate-determining step (rds) (equations (1)-(4)) [38].

$$2\ H^{+}_{(ad)} + 2\ e^{-} \rightarrow H_{2(g)} \quad (1)$$

$$Fe_{(s)} + H_2O_{(l)} \rightarrow FeOH_{(ad)} + H^{+}_{(aq)} + e^{-} \quad (2)$$

$$FeOH_{(ad)} \rightarrow FeOH^{+}_{(ad)} + e^{-} \quad \text{(rds)} \quad (3)$$

$$FeOH^{+}_{(ad)} + H^{+}_{(aq)} \leftrightarrows Fe^{2+}_{(aq)} + H_2O_{(l)} \quad (4)$$

A similar mechanism involving chemisorbed sulfide species was proposed by Shoesmith et al., as shown in equations (5) and (6) [39].

$$Fe_{(s)} + H_2S_{(aq)} + H_2O_{(l)} \rightarrow FeSH^{-}_{(ad)} + H_3O^{+}_{(aq)} \quad (5)$$

$$FeSH^{-}_{(ad)} \rightarrow FeSH^{+}_{(ad)} + 2\ e^{-} \quad \text{(rds)} \quad (6)$$

Then, $FeSH^{+}_{(ad)}$ may be hydrolyzed to yield soluble species (equation (7)), promoting the iron dissolution at low pH values [40].

$$FeSH^{+}_{(ad)} + H_3O^{+}_{(aq)} \rightarrow Fe^{2+}_{(aq)} + H_2S_{(aq)} + H_2O_{(l)} \quad (7)$$

Fig. 10 shows the variation of hydrogen oxidation current for the X70MS and X70MO steels in 0.05 mol L^{-1} H_2SO_4 + 3.0 g L^{-1} NH_4SCN solution. In the deaerated solution, both steels showed similar behavior, a slow current increase followed by a constant current (~90 μA cm^{-2}). In H_2S-saturated solutions, the current increased rapidly and then reached a steady state, however, X70MO exhibited a steady state current value significantly higher than X70MS. These current measurements are associated with hydrogen diffusivity in steel. When a direct current is applied to the working electrode, proton reduction is induced on electrode interface and then hydrogen diffuses in steel. Diffusivity depends on the size and arrangement of ferrite grains and the amount of microstructural defects and discontinuities in each steel [41,42]. After a few minutes, the hydrogen oxidation current begins to increase until it reaches a steady state. At this time, the flux of hydrogen throughout the steel remains constant. The relationship between atomic hydrogen permeation fluxes at steady state (J_{X70MO}/J_{X70MS}) [22] was approximately 1.5. It is important to mention that it is difficult to compare these results with others, as the current density depends on the experimental procedure. In this sense, the measured current increases as applied current, solution temperature, or surface roughness of the working electrode increases [42-45]. When the direct current was turned off, the hydrogen oxidation current rapidly decreased to a new steady state. This fact can be attributed to hydrogen spontaneously generated by corrosion of steel [46]. Fig. 10 indicates that the steady state current density is at least 10 times higher for steels in saturated H_2S solutions than in deaerated solutions. This ratio is in accordance with the corrosion rates. Thus, H_2S has a dual role: on the one hand, it facilitates the reduction of protons at the solution/steel interface and, on the other hand, inhibits the hydrogen gas formation reaction, favoring the diffusion of atomic hydrogen through steel.

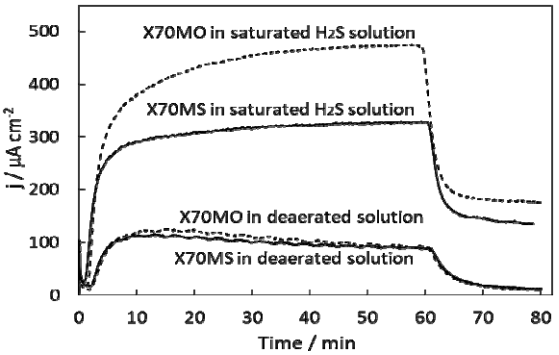

Fig. 10. Hydrogen permeation curves of X70MS and X70MO steels.

4. CONCLUSION

API 5L X70MS steel, which has a ferrite-pearlite refined microstructure, showed no cracks or blisters after HIC and SSC testing in NACE 177A solution. API 5L X70MO steel, which has coarse ferrite grains and segregation bands, failed these tests and exhibited relatively long cracks and big blisters, some of which were initiated from MnS inclusions. Both steels

showed general corrosion in this solution. From potentiodynamic measurements, it was concluded that the corrosion rate depends more on environmental factors than on metallurgical factors. In this sense, NACE 177A solution is so aggressive that the differences in composition and microstructure between steels do not seem to be important. Corrosion rate values in H_2S-saturated solution were about an order of magnitude higher than those in deaerated solution. From hydrogen permeation measurements, it was possible to reveal the effect of the microstructure on hydrogen diffusion in steel. In deaerated H_2SO_4 solution, permeation measurements were similar for both steels. This is probably due to the fact that the hydrogen permeation sites offer different resistance to diffusion. At relatively low concentrations of hydrogen atoms on the steel surface, a fraction of these sites allows the transport of hydrogen through the steel. As the concentration of hydrogen atoms on the steel surface increases, more difficult paths for diffusion are used. In H_2S-saturated H_2SO_4 solution, H_2S increased the efficiency of proton reduction at the solution/steel interface and inhibited the hydrogen gas formation reaction, favoring the diffusion of atomic hydrogen. Since X70MS steel has a more homogeneous and refined microstructure than X70MO steel, the latter offers more paths for hydrogen diffusion. Therefore, hydrogen permeation tests also confirmed that API 5L X70MO steel is not suitable for sour services.

ACKNOWLEDGEMENT

The authors would like to thank FAPESP (Process 2017/11361-5) for the financial support.

REFERENCES

1. Popoola, L. T., Grema, A. S., Latinwo, G. K., Gutti, B. and Balogun, A. S., "Corrosion problems during oil and gas production and its mitigation". Int. J. Ind. Chem., 2013, 4(35), 1-15.
2. Iannuzzi, M., Barnoush, A. and Johnsen, R., "Materials and corrosion trends in offshore and subsea oil and gas production". npj Mater. Degrad., 2017, 1, 2-11.
3. Smith, S. N., "Current understanding of corrosion mechanisms due to H_2S in oil and gas production environments". Proceeding of NACE International, (Corrosion 2015, Conference & Expo), Dallas, USA. Paper No. 5485. 2015, 7, 4567-4585.
4. Wen, X., Bai, P., Luo, B., Zheng, S and. Chen, C., "Review of recent progress in the study of corrosion products of steel in a hydrogen sulfide environment". Corros. Sci., 2018, 139, 124-140.
5. Costa e Silva, A. L. V., "Non-metallic inclusions in steels". J. Mater. Res. Technol., 2018, 7, 283-299.
6. Papavinasam, S., Doiron, A. and Revie, R. W., "Model to predict internal pitting corrosion of oil and gas pipelines". Corros., 2010, 66, 1-11.
7. Perez, T. E., "Corrosion in the oil and gas industry: an increasing challenge for materials". JOM., 2013, 65(8), 1033-1042.
8. Elboujdaini, R. and Revie, R. W., "Metallurgical factors in stress corrosion cracking (SCC) and hydrogen-induced cracking (HIC)". J. Solid State Electrochem., 2009, 13, 1091-1099.
9. Hincapie-Ladino, D. and Falleiros, H. G., "Trincamento induzido por hidrogênio em aços microligados". Tecnol. Metal. Mater. Miner., 2015, 12, 82-93.
10. Codaro, E. N., Acciari, H. A., Paula, L. J., Oliveira, M. C. and Figueredo, R. M., "A Comparative Study of Hydrogen-Induced Cracking Resistances of API 5L B and X52MS Carbon Steels". Int. J. Corros., 2018, ID 1604507, 1-7.
11. Gao, S., He, F. and Gao, J., "Corrosion problems in the oil country tubular goods and their mitigation – a review". Anti-Corros. Methods Mater., 2017, 64(5), 465-478.
12. Nejad, A. M., "A review of contributing parameters in corrosion of oil and gas wells". Anti-Corros. Methods Mater., 2018, 65(1), 73-78.
13. Neff, J., Lee, K. and Deblois, E. M., Produced Water: Overview of Composition, Fates, and Effects, eds. Lee, K. and Neff, J., Springer, New York, USA, 2011, 3-54.
14. Utvik, T. I. R., "Chemical characterisation of produced water from four offshore oil. Production platforms in the north sea". Chemosphere, 1999, 39, 2593-2606.
15. Ahmadun, F., Pendashteh, A., Abdullah, L.

C., Biak, D. R. A., Madaeni, S. S. and Abidin, Z. Z., "Review of technologies for oil and gas produced water treatment". J. Hazard. Mater., 2009, 170(2–3), 530-551.
16. Haq, A. J., Muzaka, K., Dunne, D. P., Calka, A. and Pereloma, E. V., "Effect of microstructure and composition on hydrogen permeation in X70 pipeline steels". Int. J. Hydrogen Energ., 2013, 38, 2544–2556.
17. Mohtadi-Bonab, M. A., Szpunar, A., Basu, R. and Eskandari, M., "The mechanism of failure by hydrogen induced cracking in an acidic environment for API 5L X70 pipeline steel". Int. J. Hydrogen Energ., 2015, 40(2), 1096–1107.
18. American Petroleum Institute. "Specification for Line Pipe: API Specification 5L". American Petroleum Institute, 2012.
19. TM0316, NACE Standard, "Four-Point Bend Testing of Materials for Oil and Gas Applications". NACE int., Houston, USA, 2016.
20. TM0284, NACE Standard. "Evaluation of pipeline and pressure vessel steels for resistance to hydrogen-induced cracking". NACE Int., Houston, USA, 2016.
21. ANSI/NACE TM0177. "Standard Test Method, Laboratory Testing of Metals for Resistance to Sulfide Stress Cracking and Stress Corrosion Cracking in H_2S Environments". Houston, USA, 2016.
22. ASTM G148-97. "Standard practice for evaluation of hydrogen uptake, permeation, and transport in metals by an electrochemical technique". ASTM Int., 2011, 1, 1-10.
23. Batista, G. Z., Carvalho, L. P., Silva, M. S. and Souza, M. P., "Efeito da soldagem circunferencial de tubos API 5L X65MS, X70MS e X80MS na ZAC e no metal de solda". Tecnol. Metal. Mater. Min., 2016, 13, 193-200.
24. Mohtadi-Bonab, M. A., Spzunar, J. A. and Razavi-Tousi, S. S., "A comparative study of hydrogen induced cracking behavior in API 5L X60 and X70 pipeline steels". Eng. Fail. Anal., 2013, 33, 163-175.
25. ANSI/NACE MR0175/ISO 15156-2. "Petroleum and natural gas industries – materials for use in H_2S-containing environments in oil and gas production – Part 2: Cracking-resistant carbon and low-alloy steels, and the use of cast irons", Houston, USA, 2009.
26. Rahman, K.M., Mohtadi-Bonab, M.A., Ouellet, R., Szpunar, J. and Zhu, N., "Effect of electrochemical hydrogen charging on an API X70 pipeline steel with focus on characterization of inclusions". Int. J. Pres. Ves. Pip., 2019, 173, 147-155.
27. Ma, H. Y., Yang, C., Li, G. Y., Guo, W. J., Chen, S. H. and Luo, J. L., "Influence of Nitrate and Chloride Ions on the Corrosion of Iron". Corros., 2003, 59(12), 1112-1119.
28. Sun, W., Pugh, D. V., Smith, S. N., Ling, S., Pacheco, J. L., Franco, R. J., "A Parametric Study of Sour Corrosion of Carbon Steel". Proceeding of NACE International, (Corrosion 2010, Conference & Expo), Santo Antonio, USA, Paper No. 10278, 2010, 5, 3510-3529.
29. Fioravante, I. A., Macedo, J. F., Nakazato, R. Z., Acciari, H. A. and Codaro, E. N., "A review on corrosion of low carbon steels in aqueous hydrogen sulfide". Int. J. Eng. Sci. & Res. Technol., 2019, 8(12), 1-15.
30. Fonseca, I., Proença, L. and Capelo, S., "Cyclic voltammetry and unidirectional linear voltammerty: potentialities in the study of corrosion processes". Corros. Prot. Mater., 2015, 34(1), 12-21.
31. Barnartt, S., "Tafel slopes for iron corrosion in acidic solutions". Corros., 1971, 27, 467–450.
32. Kuo, H. C. and Ken Nobe, K., "Electrodissolution Kinetics of Iron in Chloride Solutions: VI . Concentrated Acidic Solutions". J. Electrochem. Soc., 1978, 125(6), 853-860.
33. Darwish, N. A., Hilbert, F., Lorenz, W. J. and Rosswag, H., "The influence of chloride ions on the kinetics of iron dissolution". Electrochim. Acta, 1973, 18(6), 421-425.
34. McCafferty, E. and Hackerman, N., "Kinetics of Iron Corrosion in Concentrated Acidic Chloride Solutions". J. Electrochem. Soc., 1972, 119(8), 999-1005.
35. Atkinson, A. and Marshall, A., "Anodic dissolution of iron in acidic chloride solutions". Corros. Sci., 1978, 18(5), 427-439.
36. Quispe-Avilés, J. M., Hincapie-Ladino, D., Falleiros, N. A. and Melo, H.G., "A comparative investigation of the corrosion resistance and HIC susceptibility of API 5L

X65 and API 5L X80 steels". Mater. Res., 2019, 22, 1-13.
37. Bai, P., Zhao, H., Zheng, S. and Chen, C., "Initiation and developmental stages of steel corrosion in wet H_2S environments". Corros. Sci., 2015, 93, 109-119.
38. Bockris, J.O., Drazic, D., Despic, A.R., "The electrode kinetics of the deposition and dissolution of iron". Electrochim. Acta, 1961, 4, 325-361.
39. Shoesmith, D.W., Taylor, P., Bailey, M.G. and Owen, D.G., "The formation of ferrous monosulfide polymorphs during the corrosion of iron by aqueous hydrogen sulfide at 21 ^{o}C". J. Electrochem. Soc., 1980; 127(5); 1007–1015.
40. Ma, H., Cheng, X., Chen, S., Wang, C., Zhang, J. and Yang, H., "An ac impedance study of the anodic dissolution of iron in sulfuric acid solutions containing hydrogen sulfide". J. Electroanal. Chem., 1998, 451, 11-17.
41. Thomas, A. and Szpunar, J.A., "Hydrogen diffusion and trapping in X70 pipeline steel". Int. J. Hydrogen Energy, 2020, 45, 2390-2404.
42. Samanta, S., Kumari, P., Mondal, K., Dutta, M. and Singh, S.B., "An alternative and comprehensive approach to estimate trapped hydrogen in steels using electrochemical permeation tests". Int. J. Hydrogen Energy, 2020, 45, 26666-26687.
43. Li, Y., Cai, L., Liu, G. and Ma, L., "Effect of cold-rolled thickness reduction degree on characteristics of hydrogen diffusion in silicon steel". Inter. J. Corros., 2014, ID 309416, 1-5.
44. Carreño, J.A., Uribe, I. and Carrillo, J.C., "Modelling of roughness effect on hydrogen permeation in low carbon steel". Rev. Metal. Madrid. Extr., 2003, 213-218.
45. Yuan, X., "Precipitates and hydrogen permeation behavior in ultra-low carbon steel". Mater. Sci. and Eng. A., 2007, 452–453, 116-120.
46. Berkowitz, B.J. and Horowitz, H.H., "The role of H_2S in the corrosion and hydrogen embrittlement of steel". J. Electrochem. Soc., 1982, 129, 468-474.